DOI: 10.5028/jatm.2010.02010915

Juliano Fujioka Mologni*
Engineering Simulation and Scientific Software
São Paulo – Brazil
juliano.mologni@esss.com.br

Marco Antonio Robert Alves
State University of Campinas
Campinas – Brazil
marco@demic.fee.unicamp.br

Filipe Braumgratz
State University of Campinas
Campinas – Brazil
filipe.baumgratz@gmail.com

Edson Fonseca
State University of Campinas
Campinas – Brazil
edson.fonseca@gmail.com

Cesareo L. R. Siqueira
Engineering Simulation and Scientific Software
São Paulo – Brazil
cesareo.siqueira@esss.com.br

Edmundo Silva Braga
State University of Campinas
Campinas – Brazil
edmundo@fee.unicamp.br

* author for correspondence

Optimizing the e-beam profile of a single carbon nanotube field emission device for electric propulsion systems

Abstract: *Preliminary studies on field emission (FE) arrays comprised of carbon nanotubes (CNT) as an electron source for electric propulsion system show remarkably promising results. Design parameters for a carbon nanotube (CNT) field-emission device operating on triode configuration were numerically simulated and optimized in order to enhance the e-beam focusing quality. An additional focus gate (FG) was integrated to the device to control the profile of the emitted e-beam. An axisymmetric finite element model was developed to calculate the electric field distribution on the vacuum region and a modified Fowler-Nordheim (FN) equation was used to evaluate the current density emission and the effective emitter area. Afterward, a FE simulation was employed in order to calculate the trajectory of the emitted electrons and define the electron-optical properties of the e-beam. The integration of the FG was fully investigated via computational intelligence techniques. The best performance device according to our simulations presents a collimated e-beam profile that suits well for field emission displays, magnetic field detection and electron microscopy. The automated computational design tool presented in this study strongly benefits the robust design of integrated electron-optical systems for vacuum field emission applications, including electrodynamic tethering and electric propulsion systems.*

Keywords: *Electric propulsion, Carbon nanotube, Finite element analysis.*

INTRODUCTION

Field Emission (FE) cathodes consisted of Carbon Nanotubes (CNT) applied to electric propulsion systems are being developed due to their superiority over thermionic cathodes regarding power, mass and expellant consumption (Oakwa *et al.*, 2007 and Marreses-Reading, 2002). The initial studies demonstrating the outstanding performance of CNT as a cold electron field emitter were firstly reported in 1995 by (Chernozatonskii *et al.*, 1995). The highly stable crystalline structures along with high aspect ratios are the CNT's main characteristics responsible for high current density emitted and great field enhancement factors (Young, 1958). Regarding field emission phenomenon, CNTs are either arranged in a form of a film with a variety of densities and patterns, or projected as an individual CNT electron source. The first field emission experiment of a single nanotube as an electron source was reported by Rinzler *et al.* (1995) whereas the emission results followed an approximate Fowler-Nordheim (FN) behavior. Further studies on single CNTs field emitter were conducted on numerous areas, including theoretical analysis (Seidl *et al.*, 2000 and De Heer *et al.*, 1995), high vacuum experiments (Choi *et al.*, 2004) and numerical simulation (Chen *et al.*, 2007).

Understanding the fundamental CNT emission properties is necessary to design field emission systems with optimal performance. A previous work by Edgecomb and Valdre (2001) reported the electrostatic properties behavior of single CNT system as a function of the emitter aspect ratio. Besides electric field distribution and current density, the e-beam profile is an important characteristic and must be considered especially in applications involving field emission displays and electron microscopy. A highly focus e-beam shape can considerably improve the performance of field emission displays by improving their brightness and avoiding cross-talks between adjacent phosphorous cells. According to Itoh (1998) and Lei (2004), a good focusing also enhances the resolution of critical-dimension scanning electron microscopy (CDSEM) and boosts the performance of electric propulsion systems. This paper reports a numerical investigation of e-beam shape for an individual CNT field emitter operating on a triode configuration system with an integrated FG. The effects of physical design parameters and electrode voltage on the emitted e-beam shape are herein presented. Furthermore,

Received: 08/03/10
Accepted: 25/03/10

an automated computational tool was developed to numerically simulate several physical models using the finite element method (FEM).

THE FINITE ELEMENT MODEL

The ideal computational model is the one that provides the most accurate results with less complexity. Since we intend to perform simulations on a variety of scenarios, the computational process is critical and must be taken in consideration. Figure 1 shows the configuration of the device detailing the geometric variables considered on our simulations.

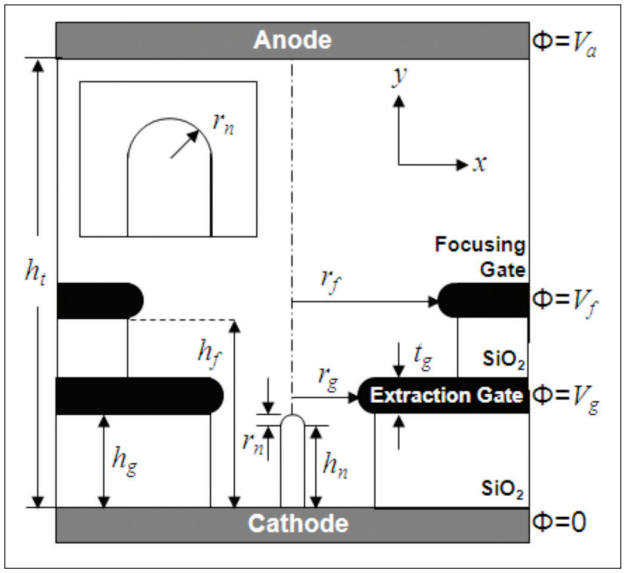

Figure 1: Cross-sectional schematic plot of the individual CNT FE system with an integrated FG. The inset image details the CNT tip radius.

Some physical parameters such as the CNT tip radius (r_n) and height (h_n), the extraction gate radius (r_g) and height (h_g), the FG radius (r_f), the gate thickness (t_g) and the distance between the cathode and anode (h_t) are assumed as constants in this study. Conventionally, the cathode voltage is grounded and is set to zero. The values of the constant parameters are shown on Tab. 1.

Table 1: Constant parameters

Parameter	r_n	h_n	r_g	h_g	r_f	t_g	h_t	V_a
Value	5	40	30	50	60	20	4	300
Unit	*nm*	*nm*	*nm*	*nm*	*nm*	*nm*	μ*m*	*V*

The FG height (h_f) is the only physical parameter considered in this study that influences the e-beam profile. The FG voltage (V_f) and the extraction gate voltage (V_g) are the electrical loads used as input variables. To investigate the effects of these variables on emitted e-beam profile is the main objective of this paper.

The positive voltage applied to the extraction gate generates an electric field that accelerates the electrons on the CNT surface toward the vacuum region via quantum tunneling. The electrons are then accelerated in the direction of the anode and their trajectories are influenced by the electric field generated by the FG.

The coaxial FG act as an electrostatic lens and control the e-beam final profile, with little participation on the emitted current density (the FG slightly affects the current emitted; some studies will be presented later on in this paper). For that reason, the aperture of the FG is always larger than the extraction gate.

Considering the nature of the geometries and loads presented in the system, one can use symmetry techniques in order to simplify the model and, therefore, reduce computational effort. It is possible to observe the rotational symmetry around the longitudinal axis of the CNT nanostructure. Mathematical calculations may be applied only on one half of the cross-sectional view and the results may be rotationally expanded. Figure 2 details the finite element model with gates rotationally expanded 180° and the CNT structure along with the cathode rotated 360°.

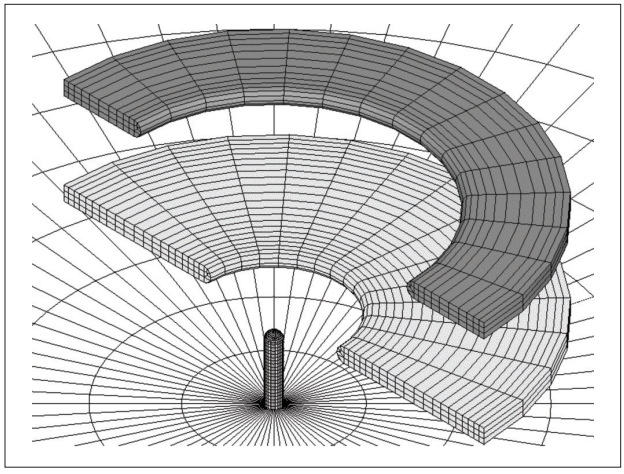

Figure 2: The axisymmetric finite element model 3D. The SiO_2 insulator layers and the vacuum mesh are omitted in this plot for a better visualization of the system. The cathode and CNT nanostructure are represented by white elements. The dark gray elements represent the FG and the light gray, the extraction gate.

NUMERICAL ANALYSIS

Considering the absence of charge-space effects and the symmetry of our model, the potential distribution (Φ) is evaluated using the following 2-D Laplace equation:

$$\nabla^2\Phi = \frac{\partial^2\Phi}{\partial x^2} + \frac{\partial^2\Phi}{\partial y^2} = 0 \qquad (1)$$

The electric field distribution is then calculated by numerically differentiating the potential distribution with respect to x and y Cartesian coordinates. Numerical and graphical results for each step of our mathematical procedure are shown on Figures 3 to 5 using the following parameters: V_f=*-10V;* V_g=*150V;* and h_f=*100nm.*

Figure 3 shows the resulting electrical potential and electric field distribution. The maximum electric field value is found at the CNT tip surface and is responsible for the field emission phenomena. As observed in Fig. 4, the electrical potential varies linearly at regions positioned distantly from the CNT structure. As a result, the electrons situated in this region flow linearly toward the anode surface. The developed tracing algorithm considers only two forces acting over the electron trajectories in this area: the electric field generated by the anode voltage and the electron inertial forces previously acquired by the extraction gate and FG electric fields.

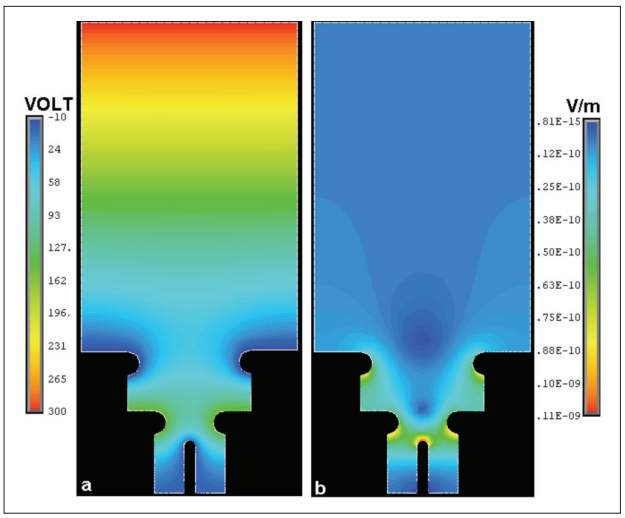

Figure 3: (a) Cross-sectional view showing the voltage contour plots on vacuum region; (b) Electric field distribution.

Using the electrostatic analysis results, one can determine the emission current density from the CNT emitter using the following FN equation (Liao *et al.*, 2007 and Niemman *et al.*, 2007), where (J) is the current density emitter ; (A) = 1.54 × 10^{-6}; (B) is -6.83 × 10^{7}; (ϕ) is the work function of the emitter in *eV*; (E) is the electric field in *V/m*, (t) can be approximated to 1; $v(y) = -0.75y^2 - 0.26y + 1.01$; and $y = 3.79 \times 10^{-4}\,(E^{0.5}/\phi)$.

$$J(\mathrm{E}) = \left(\frac{\mathrm{AE}^2}{\phi t^2(y)}\right)\exp\left(-\frac{B\phi^{3/2}v(y)}{E}\right) \qquad (2)$$

The total emitted current (I_{tip}) is then evaluated via surface integral using the electric fields values over the entire CNT surface area. A computer algorithm code was already developed for this purpose and presented by Fransen, Rooy and Kruit (1999).

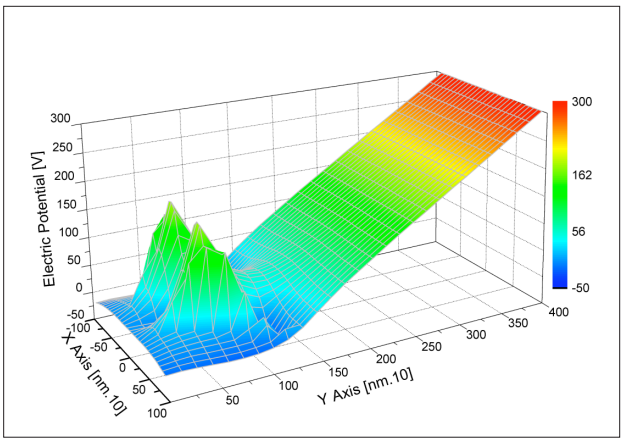

Figure 4: Spatial electric potential distribution.

$$I_{tip} = \iint_{CNT} J(E)\,ds \qquad (3)$$

Figure 5 shows the distribution of current density emission at the CNT surface. It is possible to notice that only a small effective area of the CNT tip is responsible for the emitted current. To predict the emitted electrons trajectories, we need to set the initial coordinates on the CNT surface. All nodes located on the effective emitter surface area with non-zero current density values are selected to be the initial coordinates of the electron trajectories.

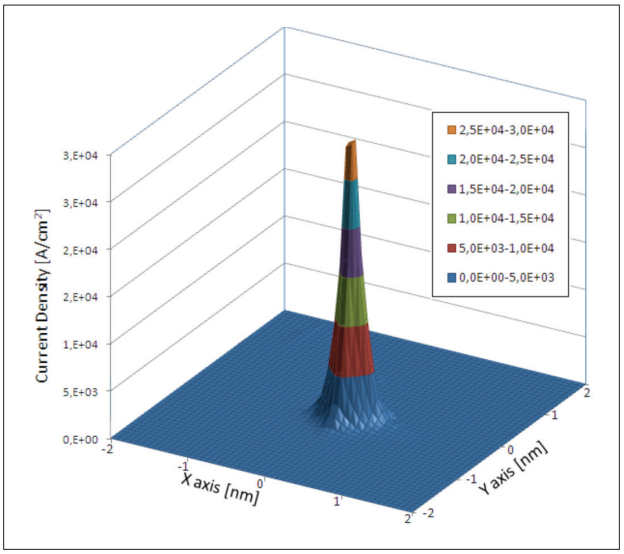

Figure 5: Surface plot showing the spatial emission current density on the surface of the CNT emitter. As expected, the maximum current density is found on coordinates *(x,y)=(0,0)*.

The projection of the electron trajectory *f(t,y)* toward the anode via vacuum is calculated according to the motion Eq. 4:

$$f(t,y) = m\{a\} = \{F\} = q\left(\{E\} + \{v\} \times \{B\}\right) \quad (4)$$

Where the mass of electron *(m)* is 9.109e-31 kg, charge of electron *(q)* is –1.602e-19 C, *{E}* is the electric field vector, *{B}* is the magnetic field vector, *{F}* is the Lorentz force vector, *{a}* is the acceleration vector and *{v}* is the velocity vector. The time integration is evaluated using the 4th order Runge-Kutta (RK) numerical method:

$$y' = f(t,y)_0 ; y(t_0) = y_0 \quad (5)$$

Where y_{n+1} is the RK4 approximation of $y(t_{n+1})$ and:

$$y_{n+1} = y_n + \frac{\alpha}{6}\left(k_1 + 2k_2 + 2k_3 + k_4\right); t_{n+1} = t_n + \alpha$$

$$k_1 = f\left(t_n, y_n\right); k_2 = f\left(t_n + \frac{\alpha}{2}, y_n + \frac{\alpha}{2}k_1\right) \quad (6)$$

$$k_3 = f\left(t_n + \frac{\alpha}{2}, y_n + \frac{\alpha}{2}k_2\right); \; k_4 = f\left(t_n + \alpha, y_n + \alpha k_3\right)$$

where *k* is the RK function and is α constant.

When located at the vacuum mesh, the electron tracing follows from element to element. The exit point of the current element becomes the entry point of a new element. The exit location and velocity for an element is obtained by integrating the equations of motion using the RK method described above. The particle tracing algorithm exploits the following assumptions:

1. No relativistic effects (electron velocity is much smaller than speed of light and the electron mass is constant).

2. The electric field within an element is constant. These simplifications reduce the computational time of the tracing algorithm.

The effectiveness of focusing is measured by the current-weighted beam radius at the anode surface. It represents the e-beam spot size (r_b) and is calculated by:

$$r_b = 2 \times \frac{\int_0^\infty J(r) r 2\pi r \, dr}{\int_0^\infty J(r) 2\pi r \, dr} \quad (7)$$

Where *J(r)* is the electron current density at the anode as a function of the distance from the azimuthal symmetry axis and *r* is the tip radius.

A computational batch process algorithm was developed and the mathematical procedures described above were performed several times with multiple input variables. The analysis output the following parameters: e-beam spot size on the anode, visual e-beam profile, current density and electric field distribution.

RESULTS AND DISCUSSION

The Response Surface Modeling (RSM) technique was used to demonstrate the dependence of each input variable (h_f, v_f and v_g) on the output result (EF_{max}, r_b). The computational automated code presented by Mologni *et al.* (2006) allows the generation of RSM on the fly, interpolating a matrix of discrete results using polynomial fit functions.

Since the additional FG was integrated to the structure to work as a focus lens only, it's reasonable to primarily investigate the influence of v_f and h_f on the current density. Based on the FN Eq. (2), one can conclude that the emitted current density is proportional to the maximum electric field value (EF_{max}) located at the tip of the emitter structure. A simulation to obtain RSM of the EF_{max} as a function of V_f and h_f was then performed.

A linear relationship between the EF_{max} and V_f for any given value of h_f is observed on Fig. 6. This is expected since all other electrical loads considered in the system are kept constant during this analysis and the space charge effect is disregarded. It is also possible to note an exponential dependence of the EF_{max} as a function of h_f. When the FG is positioned far from the extraction gate ($h_f >> h_g$), the influence of V_f on EF_{max} tends to saturate. This is explained by the high anode voltage and the great distance between the FG and the CNT emitter. If the FG is satisfactorily positioned far from the extraction gate so parallel electric potential lines between the gates can be observed, the saturation effect is achieved. The behavior of the variables presented above are only valid when we assume that V_f is applied for focusing purposes only and is very small compared to the anode and extraction gate voltages.

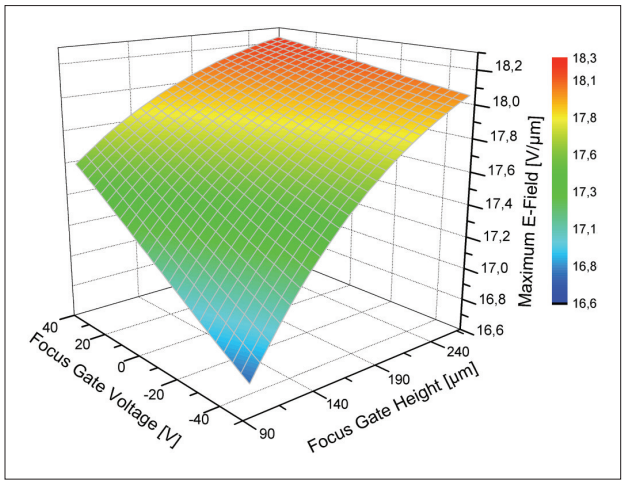

Figure 6: The dependence of the maximum electric field value on FG height and voltage.

For our study, the e-beam profiles were classified into four broadens categories:

1. No focusing – No bias is applied to the focus gate (Fig. 7a).

2. Under-focused – V_f is highly positive and attracts the electrons on the vacuum region (Fig. 7b).

3. Over-focused – V_f is negative enough to repel the electrons and at least one trajectory cross the central symmetry axis before reaching the anode (Fig. 7c).

4. Focused – The smallest r_b possible provided by the best combination of h_f and V_f (Fig. 7d).

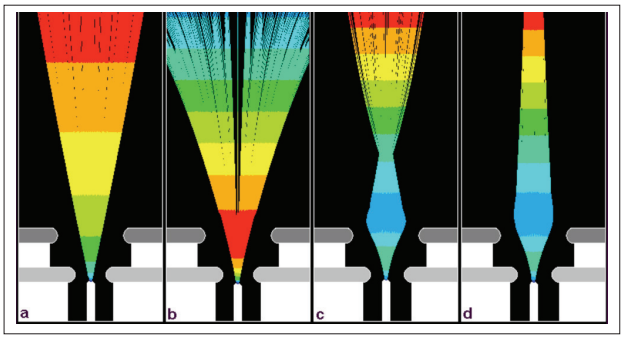

Figure 7: E-beam profile classification.

The values of trajectory, velocity and time are calculated for each emitted electron using the Lorentz Eq. (4). When a bias is applied to the FG, the electric field generated by v_f first decreases the electron velocity to adjust the trajectory and, then, accelerates the electron toward the anode. The region near the FG is considered to be a turbulent electric field region due to the variant FG electric potential. The combination of the FG and EG electric fields in this area force the electron to change its trajectory in a significant way. When the electron leaves the turbulent electric field region, the dependence of the electron velocity relies only on the anode electric field. Besides the boost on the performance of field emission displays and CDSEM, the collimation effect combined with high velocity electrons also enhances the accuracy of FE systems when they are applied to detect the presence and the strength of magnetic fields (Fig. 8).

Figure 9 shows the resulting e-beam spot size for a set of FG height and voltage values. The best e-beam weighted radius that can be achieved in this system is 15.43 nm. If necessary, additional focus gates may be integrated to the system to further increase the focusing properties. The narrowest e-beam radius can be obtained for any h_f by applying a different v_f. At highly negative values of v_f, the e-beam becomes over-focused and the value of

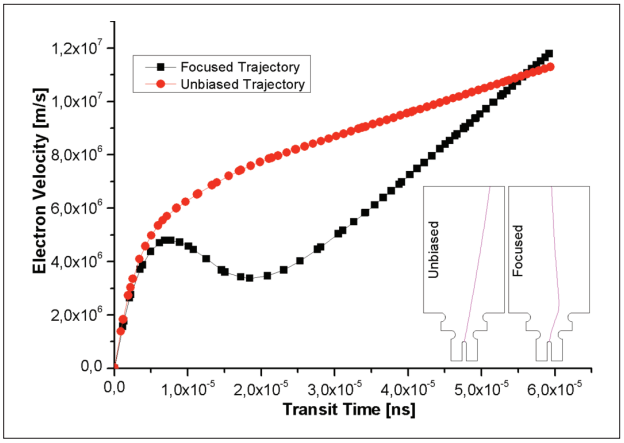

Figure 8: Electron velocity. Parameters used for this analysis: v_f=*-20 V* (for the focused electron trajectory case) and h_f=*90 nm*.

r_b increases. High values of r_b are also observed when v_f is extremely positive and the e-beam profile tends to be under-focused.

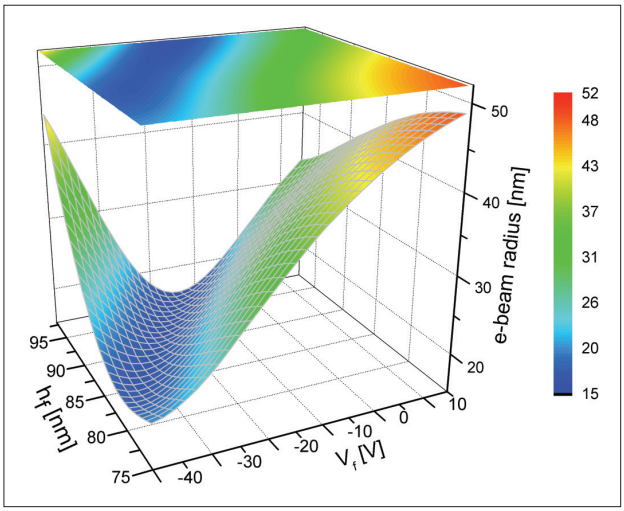

Figure 9: Effects of FG height and voltage on e-beam weighted radius on the anode.

The e-beam profile also shows a dependence on the gate electric field strength. In order to understand the e-beam weighted radius behavior for different gates biases, a simulation considering h_f constant was assumed and the results are presented in Fig. 10.

Based on Equations 2 and 3, an evaluation of the threshold voltage (when the FE system begins to emit electrons) was performed and a value of v_g=*95.43 V* was obtained. High values of r_b are found at low emission levels, when v_g is low enough to emit only a small quantity of electrons from the CNT surface. Some of these electrons are strongly repelled by the extreme negative v_f strength and present an

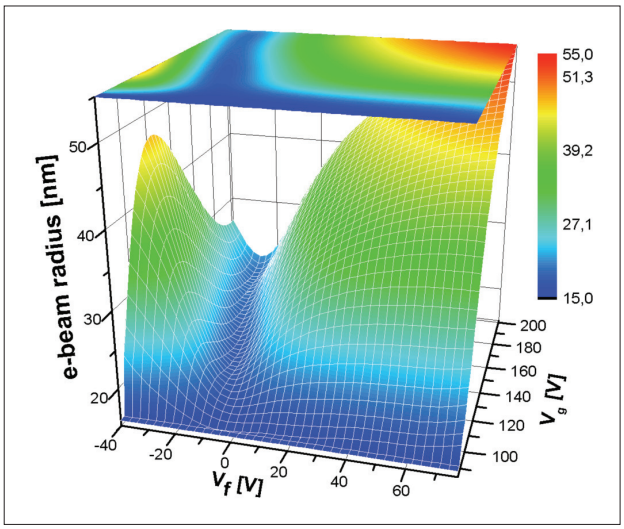

Figure 10: 3D surface plot of the e-beam weighted radius as a function of the applied gate voltages. The focus gate height was set to 90 nm for this particular case.

over-focused trajectory. On the other hand, higher values of v_f and v_g results on large r_b, but, in this case, the e-beam is comprised of under-focused electron trajectories. To correct under-focused trajectories, higher values of v_f (in magnitude) are required. It is also important to consider the increase in the effective emitter area (Fig. 5) as the v_g values raises, resulting on large e-beam profiles.

With the analysis described above, one can always modulate the biasing of the gates in order to achieve the desired e-beam weighted radius. The numerical procedure herein described may be applied to any FE system by changing the initial finite element model and carefully choosing the boundary conditions.

CONCLUSIONS

In summary, we have performed several simulations indicating the optimal FG physical and electrical parameters to achieve the best e-beam profile for a single CNT FE device regarding electric propulsion systems. An automated computational process was developed to assist the numerous simulations of diverse initial conditions. The algorithm and procedure presented in this paper can be used to simulate any geometry having at least one variable parameter. The influence of the integrated FG on the current density was also analyzed. It was shown that the presence of the FG influence the current density on the surface of the CNT emitter, especially when the FG is positioned near the extraction gate. Physical parameters of the system combined with a range of electrical loads produce a variety of e-beam profiles. The resulted profiles were determined for numerous geometric structures and the smallest e-beam spot size for a given system is achieved by using different combinations of biasing.

ACKNOWLEDGEMENT

The authors would like to acknowledge Coordenação de Aperfeiçoamento de Pessoal de Nível Superior (CAPES) and Fundação de Amparo à Pesquisa do Estado de São Paulo (FAPESP) for their support.

REFERENCES

Chen, P.Y., *et al*., 2007, "Optimal design of integrally gated CNT field-emission devices using a genetic algorithm", Nanotechnology, Vol. 18, 10p. doi: 10.1088/0957-4484/18/39/395203.

Chernozatonskii, L.A., *et al*., 1995, "Electron field emission from nanofilament carbon films", Chem Phys Lett, Vol. 233, pp. 63-68.

Choi, J.E., *et al.*, 2004, "Carbon nanotube field emitter arrays having an electron beam focusing structure", Appl Phys Lett, Vol. 84, pp. 1022-1025.

De Heer, W.A., Châtelain, A., Ugarte, D., 1995, "A carbon nanotube field-emission electron source", Science, Vol. 270, pp.1179-1180.

Edgcombe, C.J., Valdre, U., 2001, "Microscopy and computational modeling to elucidate the enhancement factor for field electron emitters", J Microsc, Vol. 203, pp. 188-194.

Fransen, M.J., Rooy, T.L., Kruit, P., 1999, "Field emission energy distribution from individual carbon nanotube", Appl Surf Sci, Vol. 146, pp. 312-327.

Itoh, J. Uemara S.K., Kanemaru S., 1998, "Three-dimensional vacuum magnetic sensor with a Si emitter tip", J Vac Sci Technol B, Vol. 16, pp. 1233-1235.

Lei, W., Yang, G., Xie, M., 2004, "Study of the triode structure in a field emission display element", J Vac Sci Technol B, Vol. 24, pp. 962-964.

Liao, K.P., Hu, Y., Lin, T.L., 2007, "Simulation studies of self-focusing carbon nanotube field emitter", J Vac Sci Technol B, Vol. 25, pp. 84-86.

Marreses-Reading, C., *et al.*, 2002, "Field emission array cathode material selection for compatibility with electric propulsion applications", Nasa JPL Technical Report, No. 8523, 17p.

Mologni, J.F., *et al.*, 2006, "Numerical study on performance of pyramidal and conical isotropic etched single emitters", Microelectronics Journal, Vol. 37, pp. 152-157.

Niemman, D.L., *et al.*, 2007, "Effects of cathode structure on the field emission properties of individual multi-walled carbon nanotube emitters", Nanotechnology, Vol. 18. doi: 10.1088/0957-4484/18/48/485702.

Okawa, Y., *et al*., 2007, "An experimental study on carbon nanotube cathodes for electrodynamic tether propulsion", Acta Astronautica, Vol. 61, pp. 989-994.

Rinzler, A.G., *et al*., 1995, "Unraveling nanotubes: field emission from an atomic wire", Science, Vol. 269, pp.1550-1553.

Seidl, A., *et al.*, 2000, "Geometry effects arising from anodization of field emitters", J Vac Sci Technol B, Vol. 2, pp. 929-932.